

Structural, Dielectric and Impedance Spectroscopy Studies of $\text{Sr}_2\text{FeNiO}_6$ nanocomposites

P. R. Padole, A. A. Jadhao, G. N. Chaudhari*

Nanotechnology Research Laboratory, Department of Chemistry,
Shri Shivaji Science College, Amravati (M.S), India
E-mail: cgnroa@yahoo.com

Abstract - The doubled perovskite $\text{Sr}_2\text{FeNiO}_6$ nanocomposite were synthesized by using sol-gel citrate method. As synthesized $\text{Sr}_2\text{FeNiO}_6$ nanocomposite were structurally characterized by X-ray diffraction (XRD) and surface morphology was studied with the help of scanning electron microscopy (SEM). XRD studies indicate that $\text{Sr}_2\text{FeNiO}_6$ have cubic structure and average crystallite size was nearly found to be ~ 22.59 nm, which is calculated with the help Scherrer equation. Fourier transform infrared spectroscopy shows the two main absorption bands at lower frequency region. Compositional features and conducting properties of $\text{Sr}_2\text{FeNiO}_6$ nanocomposite were investigated by energy dispersive X-ray spectroscopy (EDS) analysis, Impedance analysis respectively. Impedance analysis shows the presence of mostly bulk resistive (grain) contributions which is found to decrease with the increase in temperature. It suggests about the negative temperature coefficient of resistance (NTCR) type behavior of the materials. The frequency-dependent dielectric properties of the sample were investigated in the temperature range $30^\circ\text{C} - 700^\circ\text{C}$ and in a frequency range of 42 Hz – 0.5 MHz.

Keywords - $\text{Sr}_2\text{FeNiO}_6$; Nanocomposites; Sol-gel citrate; Dielectric; NTCR; EDS.

1. Introduction

Perovskites and perovskite-related oxides are known to possess a rich variety of magnetic, electrical, optical and catalytic properties. Depending on the elements, perovskites can present ferromagnetic, antiferromagnetic, diamagnetic and spin-glass properties whilst the conductivity can vary from insulation to superconductivity. More recently, perovskites have gained attention as ionic and mixed conductors for solid-oxide fuel cell (SOFC) applications as electrodes and electrolytes.

The origin of the wide interest in transition metal perovskites dates back to the discovery of high-temperature superconductivity in perovskite-related copper oxide in mid the 1980s. The efforts to improve the superconducting properties lead to the discovery of another fascinating phenomenon, colossal magnetoresistance (CMR) and later on, tunnelling magnetoresistance (TMR). In terms of chemistry, all of these materials contain the transition metal involved, Cu, Mn, Co or Fe, in a mixed valence state. Establishing the ways to control the metal oxidation states enables the preparation of new related materials. The uses for these materials are based upon their intrinsic dielectric, ferroelectric, piezoelectric, and pyroelectric properties of relevance in corresponding electronics applications such as electromechanical devices, transducers, capacitors, actuators, high-k dielectrics, dynamic random access memory, field effect transistors, and logic circuitry [1-4].

Perovskite oxides are commonly known for their ability to absorb and de-absorb oxygen reversibly. Even though this is one of the phenomena used to modify the metal valence states, it simultaneously makes the perovskites good candidates for oxide ion conductors in intermediate temperature SOFCs and oxygen sensors.

In addition to the interesting properties and potential applications of perovskites, the structural aspects have also offered their own branch of research. Especially in complex perovskites, the local environment and distribution of cations and anions control the properties of the material. As the perovskite units are commonly distorted in different ways, each new compound can act as a challenging target [5].

Some of the oxides of the double perovskites family $A_2B'B''O_6$ (A is an alkaline earth; B', B'' are heterovalent transition metals) The B-site ordered double-perovskite (DP) structure of the compounds, $A_2B'B''O_6$, is derived from that of the single-perovskite (SP) compounds, ABO_3 , upon co-occupation of the octahedral cation site with two different metal species, B' and B'', in an ordered manner, such that each $B'O_6$ octahedron is surrounded by six corner-sharing $B''O_6$ octahedra, and vice-versa.

Some compounds with ordered perovskite structure show a considerable distortion with ratio between cell parameters $c/a > 1$ which depends on the radius of the A-site cations and/or of a Jahn–Teller effect. These structural distortions have important effects on the physical properties of perovskite compound, particularly its electric and magnetic properties. Recently, motivated by the theoretical and experimental studies, it was studied the room temperature to low temperature structural and magnetic properties of the series A_2MnWO_6 (A = Ca, Sr, Ba) [6-10]. Nickel containing perovskites have been suggested as possible materials for reduced dielectric constant substrates for high-temperature superconductors and even as possible high-temperature superconductors themselves [11].

In this paper we attempt to synthesize Sr_2FeNiO_6 double perovskite nanocomposites by sol-gel citrate method. As synthesized sample was characterized, structurally and electrically was to check its applicability for SOFC.

2. Experimental details

2.1 Synthesis method

The Sr_2FeNiO_6 double perovskite nanocomposites were prepared by using sol-gel citrate method. The stoichiometric mixture of Strontium nitrate [$Sr(NO_3)_2$], Ferric nitrate [$Fe(NO_3)_3 \cdot 9H_2O$] and Nickel Nitrate [$Ni(NO_3)_2 \cdot 6H_2O$] magnetically stirred with citric acid as a chelating agent and ethanol at $80^\circ C$ for 3 hrs to get homogeneous mixture. Then it was further heated at about 130° for 12 hrs in pressure vessel to get gel precursor. Then it was subjected to 3hrs heat treatment at $350^\circ C$ in muffle furnace. After heat treatment it milled to a fine powder. The dried powder sample was calcined in the range of $350^\circ - 650^\circ C$ in order to improve the crystallinity of material.

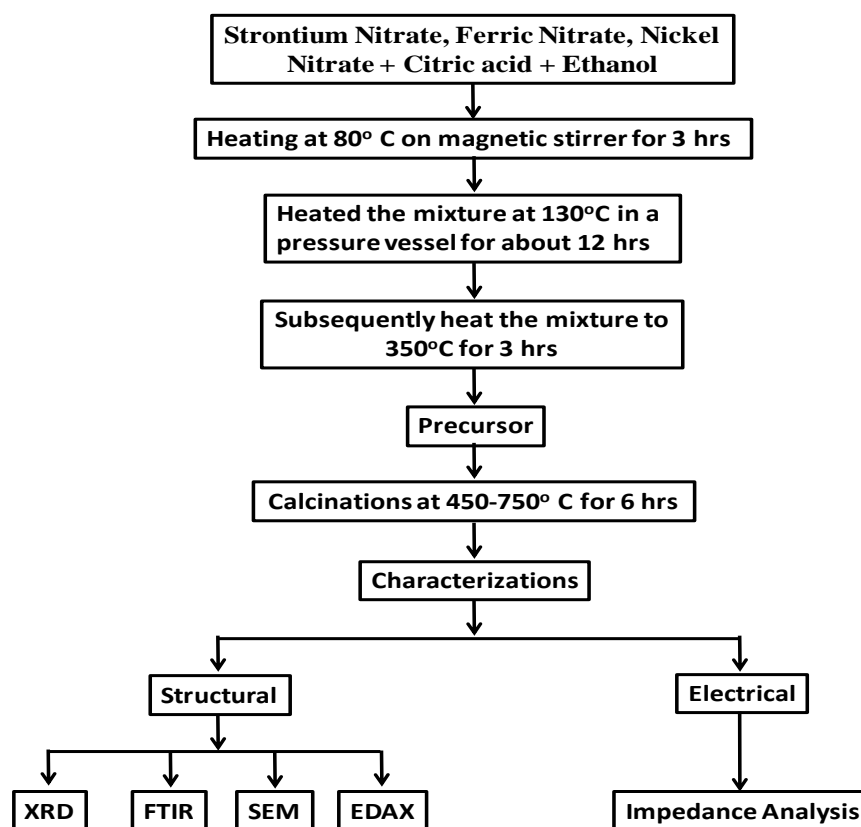
Fig.1. Shows systematic representation of preparation of $\text{Sr}_2\text{FeNiO}_6$ double perovskite nanocomposites.

Fig. 1 Flow chart for the preparation of $\text{Sr}_2\text{FeNiO}_6$ double perovskite nanocomposites.

2.2 Characterization

The structure and crystallite size of $\text{Sr}_2\text{FeNiO}_6$ nanocomposites have been investigated using Rigaku X-ray diffractometer with $\text{Cu-K}\alpha$ radiation. Samples were scanned through an angle of 20° – 70° at a scanning speed of 2.9×10^{-4} rad/s. surface morphology studies have been investigated by Field emission scanning electron microscopy (FE-SEM). Field emission scanning electron microscopy (FE-SEM) images were of the representative sample ($\times 40.1$) and were obtained using a TESCAN and MIRAILMH microscope. The composition was determined by Energy Dispersive X-ray Spectroscopy. Electrical Characterization were carried out in the temperature range Room temp - 700°C Using LCR HI-Tester (HIOKI 3532-50).

3. Results and Discussions

3.1. Structural analysis

3.1.1. X-ray diffraction

The structure and crystallite size of $\text{Sr}_2\text{FeNiO}_6$ nanocomposites was conformed with the help of XRD. Fig.2 shows the XRD pattern of $\text{Sr}_2\text{FeNiO}_6$ nanocomposites prepared by sol-gel citrate exhibit typical reflections from (1 1 1), (0 2 1), (1 2 1), (2 1 1), (0 4 0) and (1 3 2) planes which indicate the presence of cubic structure. These diffraction lines confirm the formation of $\text{Sr}_2\text{FeNiO}_6$.

The crystallite size of $\text{Sr}_2\text{FeNiO}_6$ nanocomposites was calculated using the Scherrer's relation [12].

$$D = \frac{k\lambda}{\beta \cos\theta} \quad \dots(1)$$

Where D is the crystallite size, $k = 0.9$ is a correction factor to account for particle shapes, is the full width at half maximum (FWHM) of the peaks of all planes in the XRD pattern, λ is the wavelength of Cu target = 1.5406 \AA , and θ is the Bragg angle. The distribution of the average crystallite size $\text{Sr}_2\text{FeNiO}_6$ nanocomposites synthesized through sol-gel methods was found to be $\sim 22.59 \text{ nm}$.

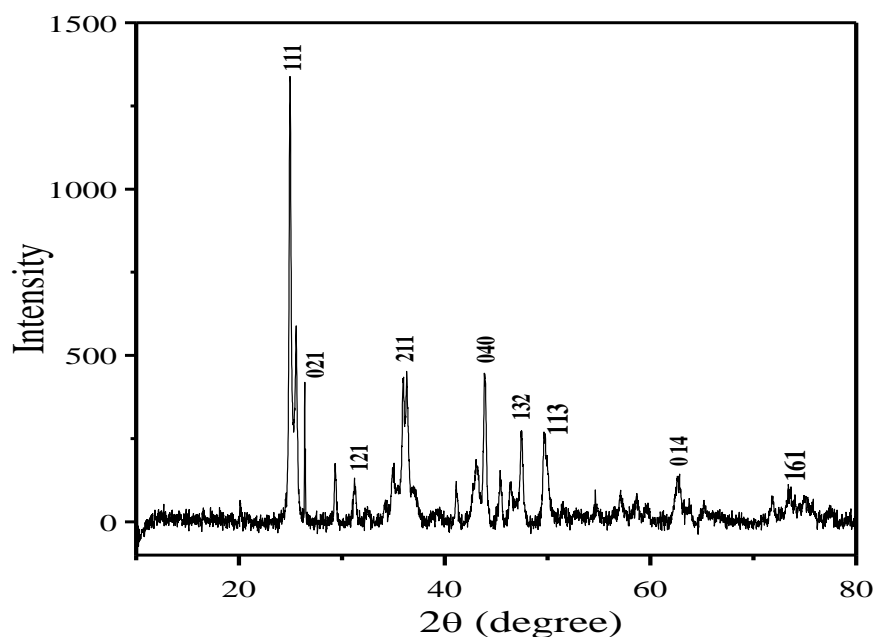


Fig. 2 X-ray diffraction pattern of the synthesized $\text{Sr}_2\text{FeNiO}_6$ calcined at 650°C .

3.1.2. FT-IR study

The formation of $\text{Sr}_2\text{FeNiO}_6$ nanocomposites was confirmed with the help of FTIR spectrum. Fig. 3 shows the FTIR spectrum of $\text{Sr}_2\text{FeNiO}_6$ nanocomposites recorded in the range of 400 to 4000cm^{-1} . The KBr technique has been used to record the spectra. Fig.3 shows The bands occurred at 420 and 702cm^{-1} are corresponding to Fe–O and Ni–O bonds respectively. The band at 1465cm^{-1} corresponds to asymmetric NO_3 stretching and a band at 1770cm^{-1} corresponds to traces of NO_3^- ions.

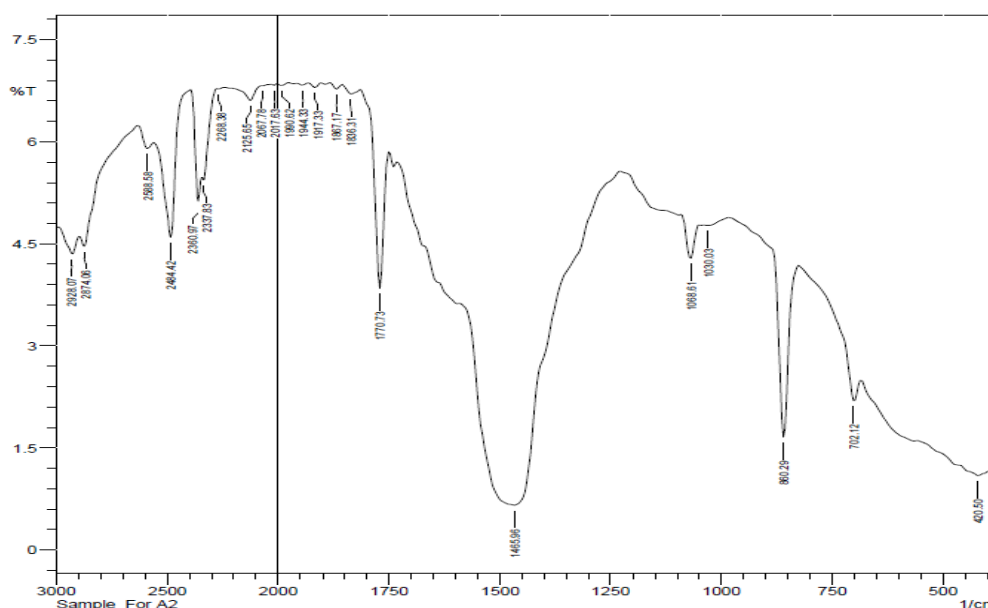


Fig. 3 The FTIR spectrum of $\text{Sr}_2\text{FeNiO}_6$ nanocomposites calcined at 650°C

3.1.3. Scanning electron microscopy (SEM) Analysis

Fig. 4 shows the structural morphology of the $\text{Sr}_2\text{FeNiO}_6$ nanocomposites, which was investigated through FE-SEM. FE-SEM picture shows that the $\text{Sr}_2\text{FeNiO}_6$ nanocomposites prepared by sol-gel method are uniform with some agglomeration of the nanoparticles were observed. The size of the particles, determined from the FE-SEM micrograph is in the order of 20–25 nm. These values of particle size are in good acceptance with the particle size calculated by Scherrer's formula.

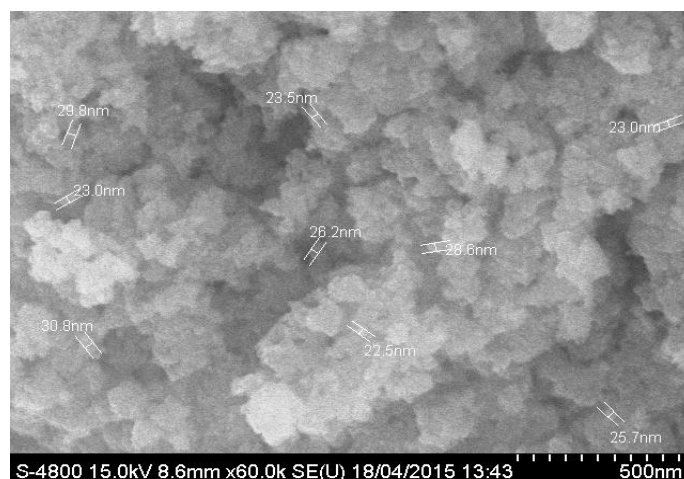


Fig. 4 SEM image of $\text{Sr}_2\text{FeNiO}_6$ DP nanocomposites.

3.1.4. Energy Dispersive X-ray (EDAX) Spectroscopy Analysis

EDAX analysis was done in order to determine the chemical composition on the surface of the sample to support our observations on the structure of $\text{Sr}_2\text{FeNiO}_6$. From fig. 5 atomic weight percentages of various cations in the as synthesized nanocomposites was found to be approximately correct which corresponds to a composition ratio and these ratios are expected.

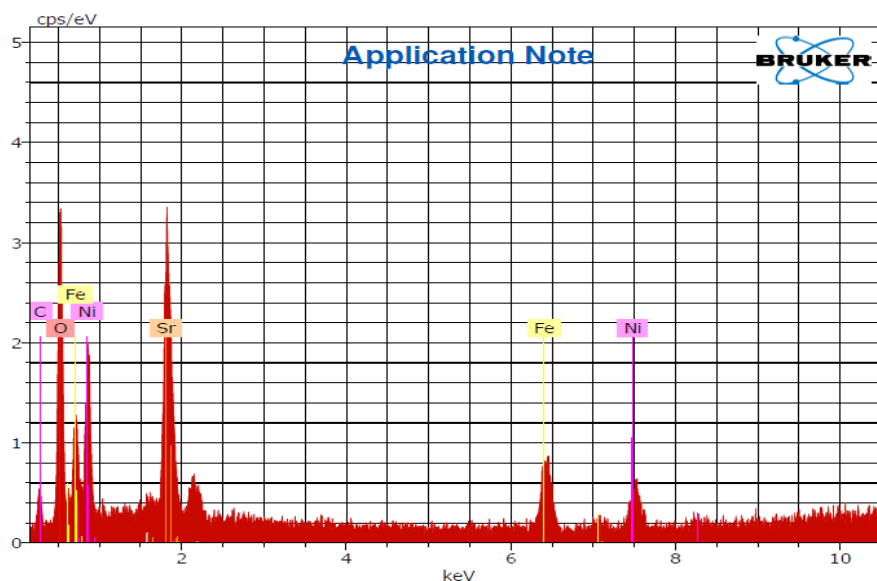


Fig. 5 EDAX pattern of Sr₂FeNiO₆ nanocomposites

3.2. Electrical conductivity

3.2.1. Dielectric constant

Study of dielectric constant (ϵ') were carried out using an ac impedance analyzer. The variation of dielectric constant with temperature is shown in fig 6. From graph it is observed that at lower frequency the Dielectric constant of the nanocrystalline Sr₂FeNiO₆ sample calcinated at 650°C is varies but with increase in frequency the Dielectric constant of the nanomaterial is nearly same and it is increases with the increase in temperature. This is due to the thermal activity and mobility of the electrical charge carriers apropos to the hopping or tunneling mechanism. The conduction process occurs as a consequence of electron exchange between Fe²⁺ to Fe³⁺ ions and hole exchange between Ni²⁺ and Ni³⁺ at the octahedral sites[13].

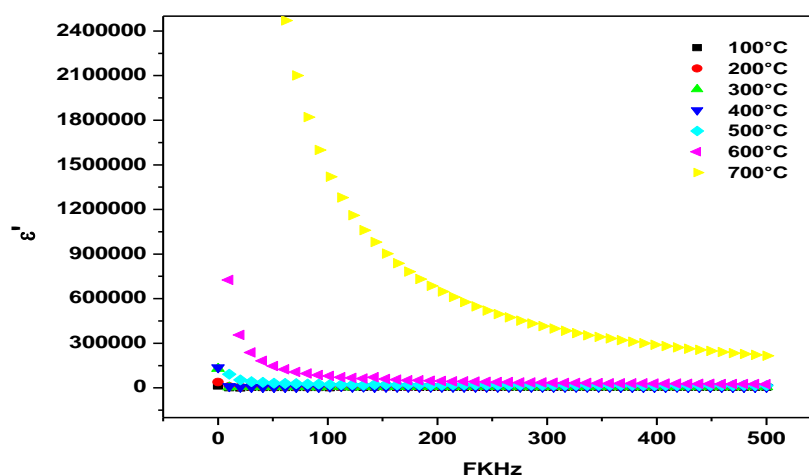


Fig. 6 Dielectric constant of the nanocrystalline Sr₂FeNiO₆ at different temperatures.

3.2.2. Impedance spectroscopy

The negative of imaginary part of impedance versus the real part of impedance plotted over a wide frequency range and at different temperatures are shown in Fig. 7. It shows that only one semicircular arc has been obtained at low as well as at high temperatures and the diameter of semicircular arc becomes smaller with increasing temperature, referring to pronounced increase in dc conduction. It shows the predominating influence of the grain boundary impedance over the entire temperature range.

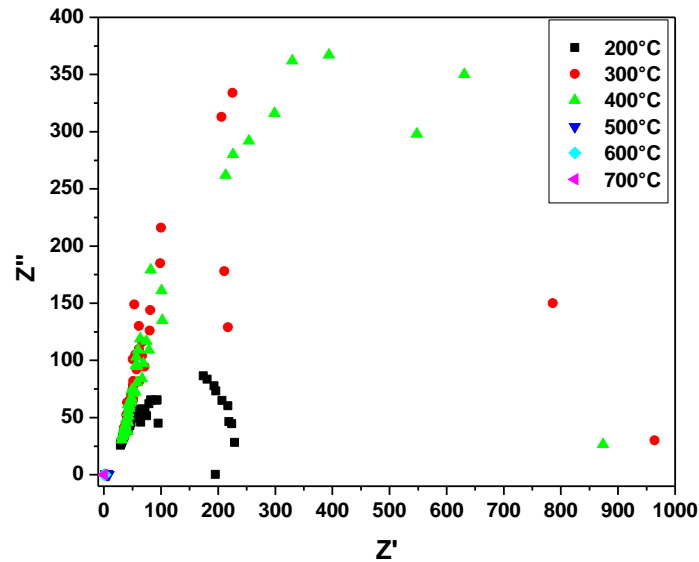


Fig. 7 Complex impedance spectra of the nanocrystalline Sr₂FeNiO₆ at different temperatures.

3.2.3. Ac conductivity

The ac conductivity (σ_{ac}) as a function of frequency at different temperatures was shown in fig. 8. It is evident that the plot of $\log \sigma_{ac}$ against $\log F$ gives straight lines with different slopes at high frequency range. The conductivity increases with increasing frequency and temperature. The enhancement rate is found to be higher in the relatively low temperature region. However as the frequency increases the conductivity becomes more and more frequency dependent.

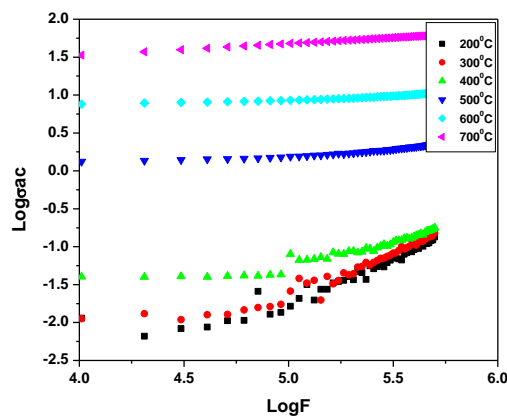


Fig. 8 Variation of ac conductivity with frequency for different temperature of Sr₂FeNiO₆.

4. Conclusions

The doubled perovskite $\text{Sr}_2\text{FeNiO}_6$ nanocomposite were synthesized by using sol-gel citrate method. XRD studies indicate that $\text{Sr}_2\text{FeNiO}_6$ have cubic structure and average crystallite size was nearly found to be ~ 22.59 nm. IR absorption spectra shows two fundamental bands ν_1 and ν_2 in the frequency range $700\text{--}400\text{cm}^{-1}$, which correspond to the tetrahedral and octahedral metal complexes, respectively. The $\text{Sr}_2\text{FeNiO}_6$ nanocomposites are uniform with some agglomeration of the nano particles were observed. The content of the metals in the double Pervoskite nanocomposites are close to the theoretical values as shown by EDAX measurements. The experimental results indicate that dielectric permittivity and ac conductivity increases as the temperature increases. Impedance measurements reveal that the impedance response is dominated by grain boundary behaviour.

References

- [1] N. A. Hill; *J. Phys. Chem.* 104, (2000) 6694.
- [2] Y. Mao, H. Zhou, S. S. Wong; *Material Matters* 5.2,(2010) 50.
- [3] A. G. Schrott, J. A. Misewich, V. Nagarajan, R.Ramesh; *Appl. Phys. Lett.* 82, (2003), 4770.
- [4] S. Tao, J. T. S. Irvine.; *Nat. Mater.* 2, (2003), 320.
- [5] D.K. Mahato ,A. Dutta,T. P. Sinha; *J Electroceramics* 29, (2012) 99-105
- [6] A. K. Azad, S. A. Ivanov, S. G. Eriksson; J. Eriksen, H. Rundlöf, R. Mathieu, P. Svedlindh; *Mater. Res. Bull.* 36, (2001), 2485.
- [7] A. K. Azad, S. A. Ivanov, S. G. Eriksson; J. Eriksen, H. Rundlöf, R. Mathieu, P. Svedlindh; *J. Mag. Magn. Mat.* 237, (2001), 124.
- [8] A. K. Azad, S. A. Ivanov, S. G. Eriksson; J. Eriksen, H. Rundlöf, R. Mathieu, P. Svedlindh; *Mater. Res. Bull.* 36, (2001), 2215.
- [9] A. K. Azad, S. A. Ivanov, S. G. Eriksson; J. Eriksen, H. Rundlöf, R. Mathieu, P. Svedlindh; *Ferroelectrics*, 269, (2002), 105 .
- [10] F. Zhao, Z. Yue, Z. Gui, L. Li; *Japn. J. Appl. Phys.* 44, (2005), 8066.
- [11] I. A. Gorodea , F. G. Brezeanu, S. Triki, K. Popa, A. R. Iordan, M. N. Palamaru, A. Simion; *Acta Chemica IASI*, 17, (2009), 49-58.
- [12] C. Hammond, *The Basics of Crystallography and Diffraction*, Oxford University Press, Oxford, 1997.
- [13] Mohd. Hashim , Alimuddin , S. E. Shirsath , S. S. Meena , R. K. Kotnala , A. Parveen , A. S. Roy, S. Kumar, P. Bhatt, R. Kumar; *J. Magnetism and Magnetic Materials* 341, (2013), 148-157.